# Characteristics of the plasma environment for the SMART-1 mission

**H. Laakso and B. Foing**
*ESA Space Science Department*
*Noordwijk, The Netherlands*

ABSTRACT

The primary objective of the SMART-1 mission is to test the performance of an electric propulsion engine in space. For the first six months, the satellite will orbit in the inner magnetosphere, spending a considerable amount of time in the radiation belt where relativistic particles can cause serious internal damage to the vehicle. When being outside that region, the spacecraft will primarily move in the nightside near-Earth magnetotail where energetic particle injections can frequently occur during magnetic substorms; both internal and surface discharging events are possible during those events. In the later part of the mission, the apogee of the trajectory moves into the solar wind, which is usually not a hostile environment to the vehicle. After nine months, SMART-1 will be inserted into a polar orbit around the Moon. When moving into the optical shadow of the Moon, the spacecraft may assume quite negative potentials, up to a few hundreds of volts if the Moon is in the solar wind, and up to several thousands of volts if the Moon is in the distant magnetotail.

## 1. INTRODUCTION

The ESA has introduced a new series of small satellites, called SMART (Small Mission for Advanced Research and Technology), that are intended to test new technologies in space. The primary objective of SMART-1 is to demonstrate the performance of solar electric propulsion, by moving the spacecraft into a polar orbit around the Moon. The engine selected is a stationary plasma Hall-effect thruster, the PPS-1350, developed by SNECMA, that uses Xenon gas as propellant. The power for the engine is taken from the spacecraft's solar arrays, and as a result, the thruster will accelerate the vehicle with a force of about 70 mN.

The SMART-1 satellite will carry seven experiments, conducting nine investigations in total (see Table 1). Some of the instruments (EPDP, RSIS, SPEDE) are dedicated to monitoring the performance of the propulsion engine. The scientific objective of the SMART-1 mission is to explore the lunar surface, by monitoring lunar chemical elements (D-CIXS/XSM) and surface mineralogy (SIR), and doing multi-band imaging (AMIE). In addition SMART-1 carries three other investigations (Laser-Link, OBAN, and KATE) that will test and demonstrate new techniques for navigation and telecommunication in space.

*Table 1. Instruments of the SMART-1 satellite.*

| **Experiment** | **Primary objectives** |
|---|---|
| *AMIE* | 5° FOV miniaturised CCD-camera, with 4 fixed filters and micro-DPU. Moon multi-band imaging and data integration, education & public outreach. It supports demonstration of Laser-Link, RSIS and Autonomous Navigation Investigations |
| *Laser-Link Investigation* | Demonstration with AMIE images of a deep-space laser link from the ESA Optical Ground Station, and of sub-aperturing techniques for atmospheric correction |
| *OBAN Investigation* | Validation of On-Board Autonomous Navigation algorithm by planetary bodies tracking. It uses existing on-board equipment (star-trackers) and AMIE images |
| *SPEDE* | Langmuir probes on booms to measure spacecraft potential, electron and plasma environment. Support to Electric Propulsion monitoring |
| *RSIS Investigation* | Radio-science experiments to monitor the Electric propulsion and to test a novel method to measure rotational properties of a planetary body from orbit (verification on Moon libration). It uses KATE and AMIE on-board instruments |
| *SIR* | Miniaturised Near IR (0.9–2.4 μm ) monolithic Grating point-spectrometer, for lunar surface mineralogy studies |
| *D-CIXS* | Compact X-ray spectrometer based on Swept Charge Detectors and μ-collimator: mapping of lunar chemical elements |
| *XSM* | X-ray variations of sun and cosmic sources, and solar X. Calibration for D-CIXS |
| *EPDP* | Multi-sensor package for monitoring the Electric propulsion, it supports SPEDE for Plasma environment characterisation |
| *KATE* | X/Ka-band TT&C package, it demonstrates telecommunication, tracking and tests turbo-codes and VLBI operation. It supports the radio-science experiments (RSIS) |

## 2. SMART-1 ORBIT

The SMART-1 satellite will be launched as auxiliary payload by Ariane-5, in a one year launch splot, starting at the end of 2002. The satellite will first be delivered into a geostationary transfer orbit (with the perigee of 6,962 km, apogee of 42,164 km, inclination of 7°). After commissioning period, the solar electric propulsion will be switched on, and the spacecraft will start its 9-month spiralling trajectory to escape the Earth gravitational field. The thrusting will be almost continuous during the first two months to minimize damage from the inner radiation belt. The spacecraft will be thrusted in two modes where the orbit absides increase and the orbit inclination is changed.

About 9 months after the launch, the spacecraft will be inserted into a lunar orbit with the perigee of 2,738 km, apogee of 11,738 km, and inclination of 90°. For the following 21 days, the trajectory is lowered, by means of the solar electric propulsion engine, to the final orbit with the perigee of 1,000 km, apogee of 10,000 km, inclination of 90°, and orbital period of 15 hours. Then the lunar overall nominal observation phase begins, lasting six months, during which the Moon will be monitored from more than 200 orbits.

Figure 1 shows the orbit of the SMART-1 satellite in the xy plane of a geocentric coordinate system (GSE), where the x axis points to the Sun, the y axis is in the ecliptic plane, pointing duskward, and the z axis completes the frame, pointing to the northern ecliptic pole. The paraloid represents the average location of the magnetopause, under the mean solar wind conditions; the circle is at a geocentric distance of 8 Earth's radii and is approximately the outer edge of the radiation belt. Thus, for the beginning of the mission, the satellite will orbit in the radiation belt and in the near-Earth magnetotail. Later, the satellite will move towards the dayside magnetosphere and will linger a substantial amount of time in the solar wind before it will be captured by the Moon. The satellite will then orbit around the Moon for six months, during which the vehicle, together with the Moon, will encounter the distant magnetotail six times.

## 3. EFFECTS OF THE PROPULSION SYSTEM

The solar electric propulsion system may well change the plasma environment around the vehicle and also cause some effects on the satellite. Therefore, monitoring of the plasma environment near the spacecraft is one of the primary objectives for two experiments: SPEDE and EPDP. The numerical simulations by *Tajmar et al.* [2001] show that the effects are not expected to be significant but an operating engine can increase the plasma density well above the ambient density of a tenuous magnetosphere. For instance, outside the plasmasphere, the plasma density drops quickly below 1 $cm^{-3}$ [*Laakso and Jarva*, 2001], and in the tail lobes and auroral cavities the density is usually of the order of 0.01 $cm^{-3}$. In such an environment, the satellite usually floats at a very positive potential, even above +60 volts.

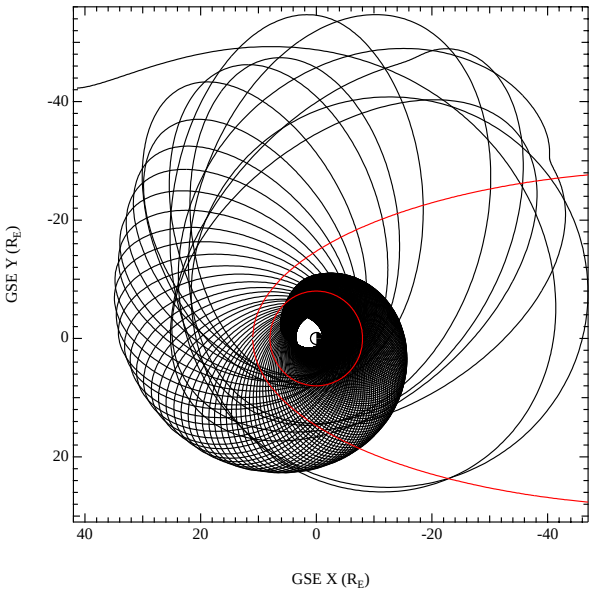


*Figure 1. Trajectories of the SMART-1 satellite in the GSE xy plane for nine months after the launch; a paraboloid shows the mean magnetopause location and a circle represents the outer edge of the radiation belt (assumed launch date: Dec 2002).*

A fundamental question about the performance of propulsion is whether any part of the exhaust gases will accumulate on the satellite surface. This issue will be investigated by the SPEDE and EPDP experiments. *Laakso et al.* [2001] have studied a similar problem on the Vega spacecraft during the comet Halley encounters. The vehicles carried an infra-red camera that was cooled down with a cold neutral gas beam. It was found that the gas injections were well collimated but nevertheless rather strong disturbances and contamination effects took place. Also, the perturbations did not vanish when the gas injections were turned off but they continued at least for a few hours more.

Therefore one question is that if some gas accumulation will develop on the satellite surface, how long the contamination effects persist. *Brace et al.* [1988] studied the variation of the photoelectron current from a negatively biased Langmuir probe in the Venus atmosphere/ionosphere. They found that in the dense planetary atmosphere, the photoelectron yield of the surface is quite low because the surface can hold many monolayers of heavy atmospheric constituents, decreasing the photoemission

current. When the satellite moved into the solar wind, ion sputtering removed such monolayers, in about 100 days.

## 4. EARTH'S MAGNETOSPHERE

According to Figure 1, SMART-1 will spend a considerable amount of time in the near-Earth magnetosphere. Figure 2 shows a detailed plot of the SMART-1 orbit for the first six months; a circle is at a geocentric distance of 8 Earth's radii, representing the outer edge of the radiation belt, and a paraboloid shows the average location of the magnetopause, the outer edge of the magnetosphere, under the mean solar wind conditions. One can notice immediately that the satellite will be either in the radiation belt or in the near-Earth magnetotail, which is always a concern to any mission because both regions can be detrimental to the vehicle and its instruments.

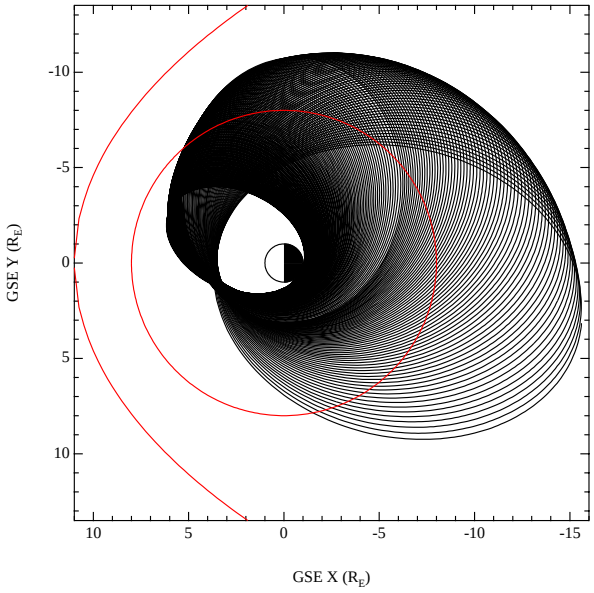


*Figure 2. SMART-1 orbit for the first six months after the launch*

Our knowledge about the dynamics of the radiation belt has significantly improved during the past decade because of long-term studies of the relativistic particles monitored by the SAMPEX and POLAR satellites [e.g., *Baker et al.*, 1999; *Kanekal et al.*, 1999]. For an example, the annual variation of the relativistic (2–6 MeV) electrons in 1999 is shown by Figure 3. Large enhancements in the electron flux are common and appear quite frequently, practically with no relationship to a solar cycle. They occur during magnetic storms that, on the other hand, tend to happen quite constantly, for instance, as a consequence of CME and other solar disturbances [see e.g., Figure 1 in *Baker et al.*, 1999]. The relativistic particles do not play any role in surface charging but penetrate through the surface, causing internal discharging events [*Soubeyran*, 1996].

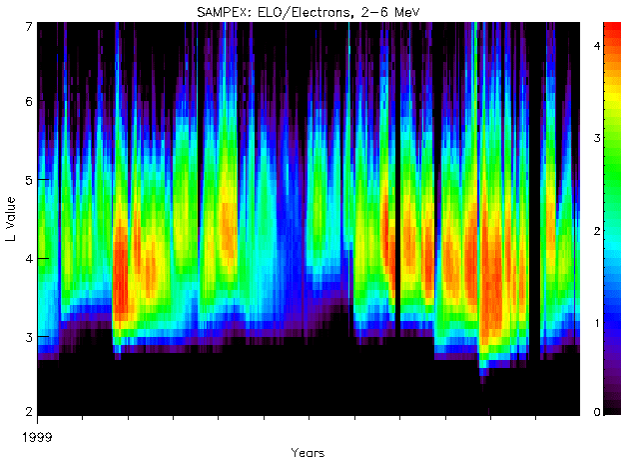


*Figure 3. Relativistic (2-6 MeV) electron flux measured by SAMPEX in year 1999. Left axis shows the L shell of the satellite, bottom axis the number of day in 1999. (Courtesy of S. Kanekal, University of Maryland).*

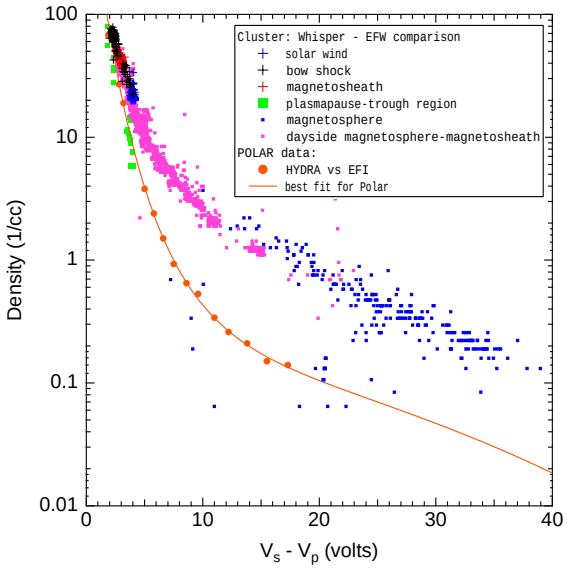


*Figure 4. Ambient plasma density plotted against satellite potential*

In the early part of the mission, SMART-1 will often be immersed in the near-Earth magnetotail (the plasma sheet or the neighbouring tail lobes) where high level surface and internal charging may develop. Due to a low ambient plasma density and a high photoemission current, the satellites usually float at a high positive potential in these regions. Figure 4 shows empirical data for the relationship between the total plasma density and the satellite potential. On the Cluster satellites, the densities were determined by the Whisper experiment (an active sounding instrument) [for more details, see *Decreau et*

*al.*, 2001] and the satellite potential by the electric field experiment EFW [for more details, see *Gustaffson et al.*, 2001]. On the Polar satellite the measurements were collected by the HYDRA and EFI experiments [for more details, see *Scudder et al.*, 2000]. The data points from Cluster and Polar deviate clearly from each other, possibly by reason of different characteristics of the surface materials. Notice also that the data points do not fit to a line because the photoelectron flux consists of multi-Maxwellian electron populations: the satellite potential below 5 eV is controlled by a low-energy photoelectrons, whereas the potential variation above that depends upon the characteristics of the high-energy photoelectrons [for more details, see *Laakso and Pedersen*, 1994].

Figure 5 sketches the main regions of the magnetosphere at the noon-midnight meridian with typical orbits for the Polar and Cluster satellites; the lines in the figure represent magnetic field lines. Although the inclination of the SMART-1 orbit will be much lower than those of Cluster and Polar, it will encounter similar plasma environments as Cluster and Polar, on its way to the Moon, because the characteristics of the plasma environment do not change significantly along the magnetic field lines at high altitudes.

In the outer plasmasphere where the density is typically around 100 $cm^{-3}$, the satellites assume a positive potential of a few volts. When the vehicles move outside the plasmasphere, the plasma density declines steeply, and correspondingly the satellite potential becomes increasingly positive; especially inside auroral cavities the surface potential can occasionally be more than +68 volts which is the saturation level of the spacecraft potential measurements on Cluster and Polar [*Laakso*, 2001].

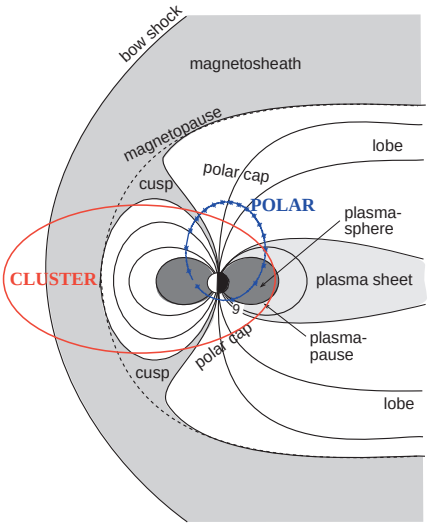


*Figure 5. Sketch of the magnetosphere with Cluster and Polar trajectories in the noon-midnight meridian.*

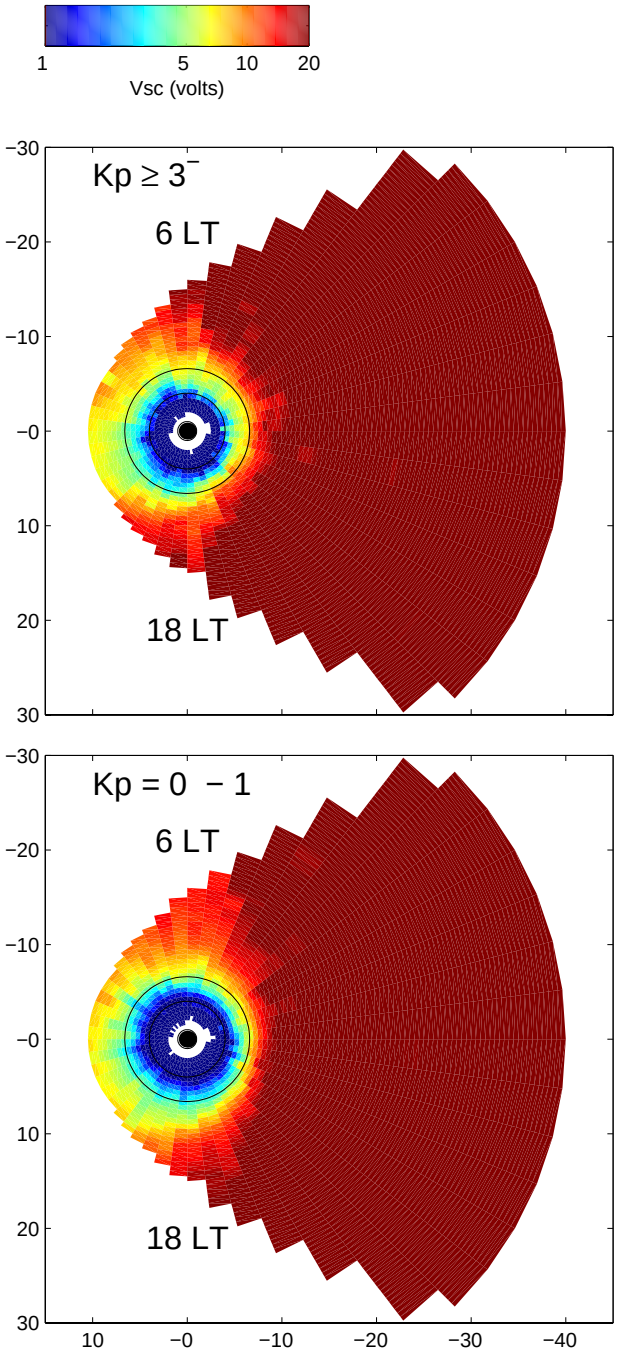


*Figure 6. Average spacecraft potential of the Polar satellite in the GSE xy plane, based upon 45 months of measurements in 1996-1999. The upper figure is for disturbed conditions, the bottom one for quiet conditions.*

Figure 6 shows statistical results on how the average satellite potential varies in the equatorial magnetosphere; the result is based on 45 months of measurements with the electric field instrument on the Polar satellite in 1996-

99 [for more details, see *Laakso*, 2001]. The bottom figure is for quiet periods (Kp index is 1 or less) and the top one for disturbed conditions (Kp is 3- or more). The two circles are at 4 and 6 Re geocentric distances. Thus, in the nightside magnetosphere the average surface potential is more than +20 volts, whereas in the dayside magnetosphere the potential is usually less than +10 volts. However, these results exclude two important cases where the satellite can become negatively charged. Firstly, when the vehicle moves into a shadow, it becomes immediately negatively charged, usually several 100 volts or more [*Garrett and Rubin*, 1978]. Secondly, when the satellite is hit by a high flux of energetic electrons, commonly occurring during a substorm, it can often become several kilovolts negative with respect to the ambient plasma [e.g., *Garrett and Rubin*, 1978; *Mullen et al.*, 1986]. Such a high-level charging event develops because for a negative surface potential, the level of charging is directly proportional to the temperature of the ambient electrons [*Laakso et al.*, 1995], which is usually in the range of keV for the nightside magnetosphere.

Figure 7 shows a typical case of how the surface potentials of the four Cluster satellites vary along their 56-hour orbits; this event is for a trajectory shown in Figure 5. The four time series overlap quite well because the satellites are separated by some 100 km only and are therefore in a similar plasma environment. A closer examination of the data can reveal some differences, however, which is beyond the scope of this paper. Figure 8 shows the first 11 hours of the interval of Figure 7 along the outbound magnetospheric orbit from the perigee into the magnetosheath. The observations deviate at 23–02 UT on 18–19 January 2001, because at that time the potentials of Cluster 2 and 4 were actively contolled by the ASPOC experiment. In Figure 8 largest voltages appear in the 50 volts range and are observed over the northern polar cap. Almost as large potentials develop in the auroral region, near 23 UT on 18 January 2001.

## 5. SOLAR WIND

The apogee of the Cluster trajectory is 19 Earth's radii, and therefore the satellites can collect interesting multipoint observations in the solar wind. Figure 9 shows a detailed plot of spacecraft potential observations gathered in the magnetosheath and solar wind regions. Particularly the electron foreshock region can be particularly turbulent with plenty of density variations, causing rapid changes in the satellite surface potential.

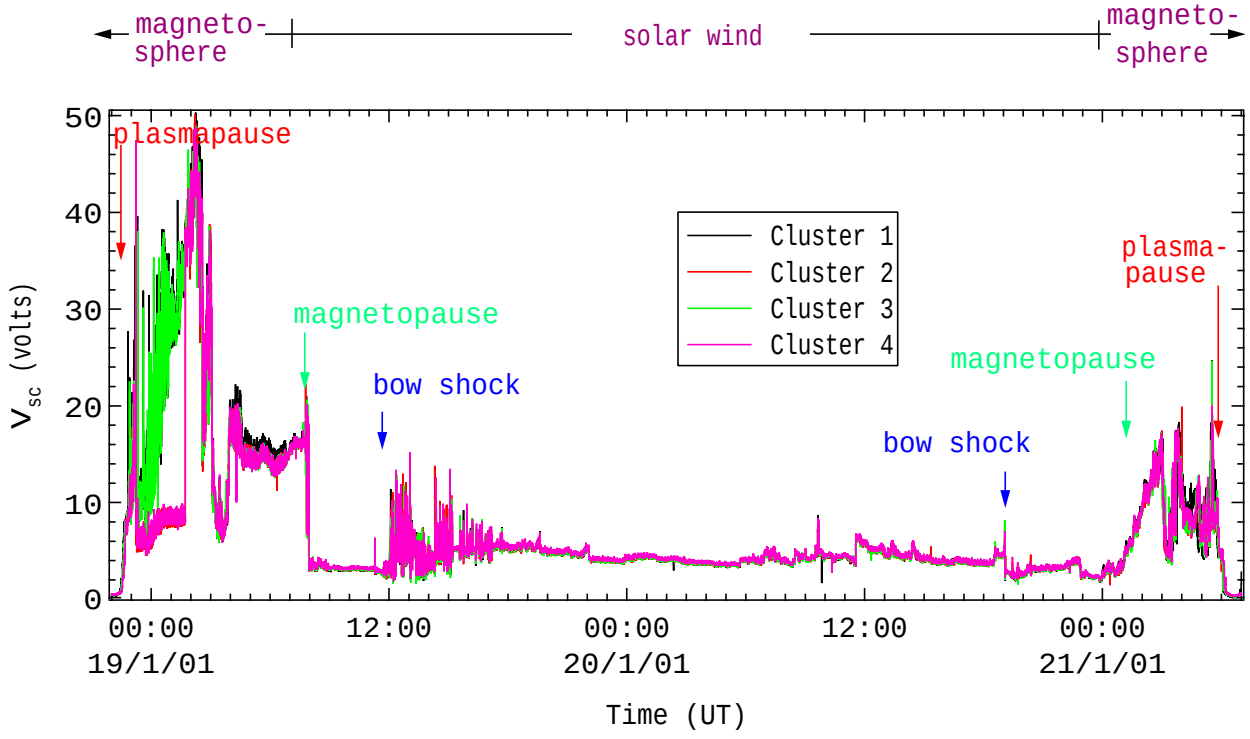


*Figure 7. Variation of the surface potential of the Cluster satellites along the trajectory of Figure 5.*

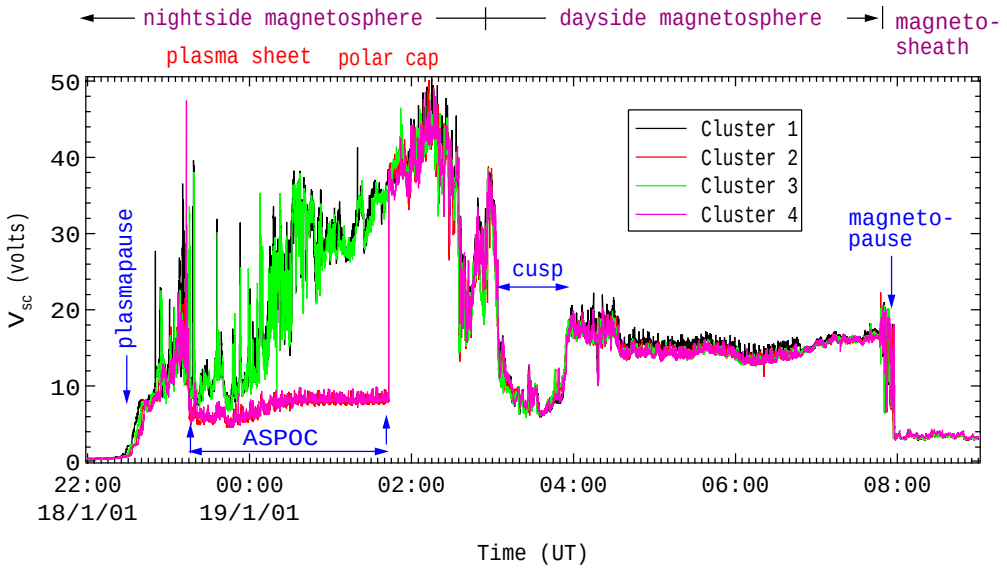


*Figure 8. Variation of the surface potential of the Cluster satellites in the magnetosphere.*

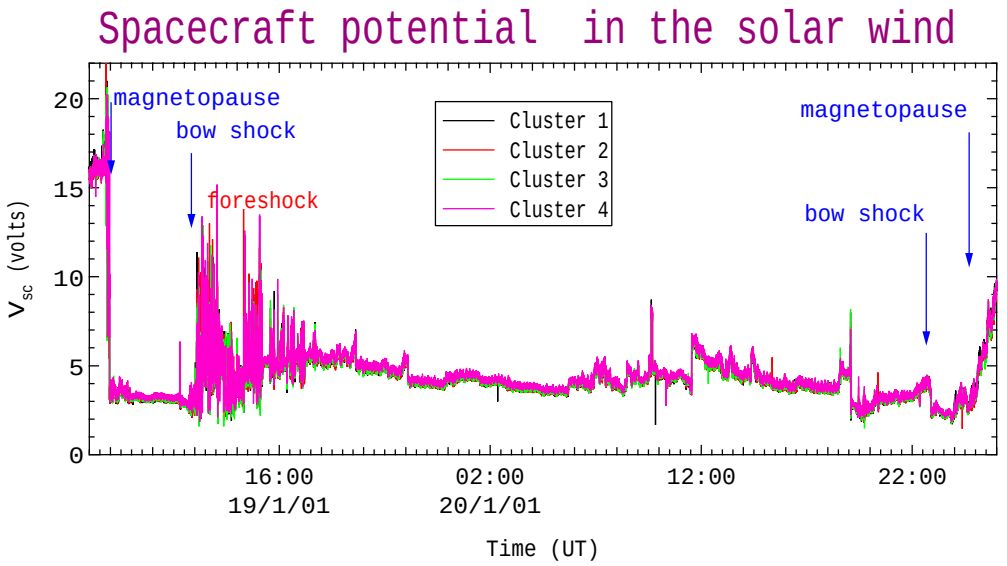


*Figure 9. Variation of the surface potential of the Cluster satellites in the solar wind.*

As a rule, the vehicles float at positive potentials between a few volts and about +10 volts in the solar wind, although occasionally much higher positive voltages have been observed. In the solar wind thermal solar wind electrons dominate the surface charging, and therefore charging is not an important issue for most of time. Occasionally the Sun injects a cloud of relativistic particles that in principle can be harmful, but their flux usually remains so low, compared to that in the radiation belt that internal charging events have not been a problem to the vehicle. However, some instruments may sometimes suffer from malfunctions during solar proton events.

## 6. LUNAR ENVIRONMENT

For the last six months of the mission, SMART-1 will be inserted into a 90° orbit around the Moon. At that time, the vehicle will encounter the optical shadow of the Moon several times, where the spacecraft charging essentially depends upon whether the Moon is in the solar wind or in the magnetosphere. This is because in shadow the surface potential is primarily proportional to the plasma temperature [*Laakso et al.*, 1995].

Although the Moon possesses no proper atmosphere or no internal magnetic field, its interaction with the solar wind is quite interesting. The sunlit surface of the Moon usually assumes a positive voltage of less than +10 volts, if the Moon is immersed in the solar wind [*Grobman and Blank*, 1969]. When being in the magnetosphere the lunar dayside surface may end up into higher positive voltages due to a low ambient electron flux. On the other hand, then the potential of the nightside sector is controlled by tail particles only, and the surface potential can easily be charged very negative, up several 1000 volts.

When the Moon is in the solar wind, a lunar environment is characterized by a wake in the nightside sector [for details, see e.g. *Spreiter et al.*, 1970], because the solar wind ion flow speed is much larger than the ion thermal speed. Therefore, the ions should flow past the obstacle and keep also the electrons away from the wake in order to fulfill the requirement of quasi-neutrality. One may ask how good the vacuum is behind the Moon. And if the ambient density is very low in the wake, one may also ponder how well the surface equilibrium potential is defined for the nightside. It is not easy to answer these questions with the limited amount of measurements available around the Moon. Good data sets of plasma observations were collected by Explorer 35 in 1967 and the Apollo missions in the 70'ies. The lunar wake was studied as well as a number of interesting features were found near the wake boundary [e.g., *Hollweg*, 1968; *Colburn et al.*, 1971; *Russell and Lichtenstein*, 1975].

More recently, the Lunar Prospector carried an electron spectrometer and a magnetometer, collecting measurements along a near-circular 100 km altitude lunar polar orbit in Jan-Dec 1998 [*Lin et al.*, 1998]. The spectrometer monitored the electron fluxes at 15 energy channels. Figure 10 shows an example of these observations along six orbits around the Moon; the electron energies for the time series from top to bottom are 40, 60, 90, 140, 220, 340, 520, 800, 1200, 1900, 2900, 4500, 7000, 11000, and 17000 eV. Steep electron flux declines are always observed in the wake in all energy channels. The fluxes decrease an order of magnitude or more in the energy channels below 200 eV. In the lowest two channels (40 and 60 eV) the diminishment is usually 2-3 orders of magnitude. One may interpret this observation as an absence of low-energy electrons in the cavity because of the formation of the wake. On the other hand, energetic electrons should be able to enter the cavity because of their large thermal velocity, but this is not supported by Figure 10. Figure 11 presents two energy spectra for the wake (blue curve) and the solar wind (red curve) regions. The wake effect appears to be largest for low and high energies. The latter observation is somewhat surprising, but may be caused by the fact that energetic electrons cannot gyrate into the middle of the wake near the lunar surface without hitting the surface somewhere; note that the observations were collected at 100 km altitude, which is rather close to the gyroradii of 5–20 keV electrons.

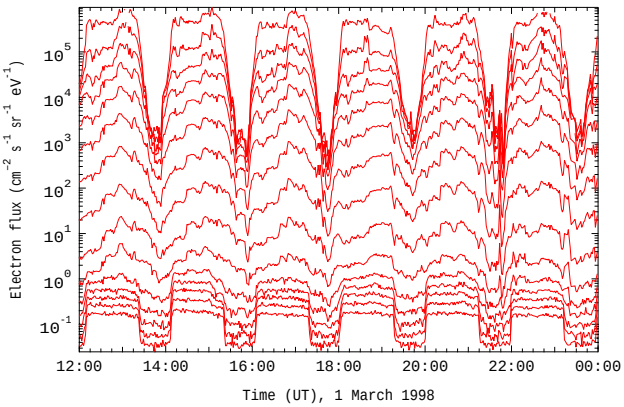


*Figure 10. Electron fluxes for 15 energy channels, measured by the Lunar Prospector, on 1 March 1998, 12–24 UT. The steep flux diminishments appear when the satellite is in the lunar wake.*

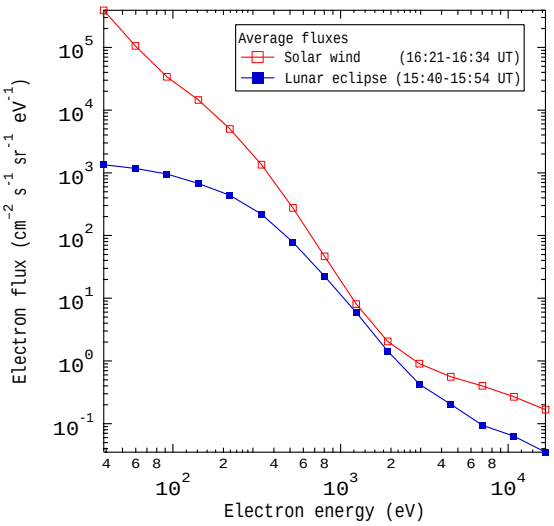


*Figure 11. Average electron flux vs. electron energy, measured in the solar wind and in a lunar eclipse, on 1 March 1998.*

For the observations of the low-energy electron fluxes, there is an important effect that needs to be taken into account in order to interpret the observations correctly. Namely, the spacecraft is charged to a negative potential in the absence of solar illumination, which prevents low-energy electrons (those whose energies are less than the surface potential of the satellite) from entering the detector that is placed only at a distance of 2.5 meters from the satellite. In the shadow the satellite should float quite negatively, perhaps several tens of volts, and therefore some of the low-energy electrons may not reach the instrument.

## 7. SUMMARY

During its 1.5-year lifetime, the SMART–1 satellite will encounter a variety of plasma environments. Some of them can be detrimental to the satellite and its payload. For instance, for the first six months, SMART-1 will orbit primarily in the radiation belt or in the near-Earth magnetotail. In the radiation belt, the serious effects are related to internal charging while the surface potential is very close to the ambient plasma potential due to a high flux of cold plasmaspheric electrons. Relativistic electron fluxes can significantly increase within a day [*Baker et al.*, 1999], as a consequence of a magnetic storm that tend to occur quite frequently from year to year, practically with no dependence upon a solar cycle.

In the magnetotail the satellite usually floats at potentials of more than +10 volts. On the Cluster and Polar satellites, the saturation of the measurements, +68 volts, is encountered occasionally. Such events are mostly related to low-density auroral cavities or to polar cap regions. In the tail harmful surface charging, i.e. large negative potentials, is primarily caused by energetic electron injections during substorms. Then the satellite can suddenly become strongly negative, up to –10 kV. The same source can also produce electrons up to relativistic energies that may cause internal discharging events.

Part of its lifetime, especially while orbiting the Moon, the vehicle will be in the solar wind and be then subject to solar disturbances (CME's etc), which can cause problems to some instruments but which are not usually a concern to the satellite itself from a spacecraft charging point of view. When being in a lunar orbit, the satellite will occasionally encounter the lunar optical shadow, during which some negative charging will occur. In fact if the Moon is in the magnetotail when it happens, very large negative surface potentials will develop.

## ACKNOWLEDGMENTS

We thank S. Kanekal for the use of Figure 3. The Lunar Prospector observations for Figures 10 and 11 were obtained via the NASA's Planetary Plasma Interactions Node of the Planetary Data System archives.

## REFERENCES

Baker, D. N., S. G. Kanekal, T. I. Pulkkinen, and J. B. Blake, Equinoctial and solstitial averages of magnetospheric relativistic electrons: a strong semiannual modulation, *Geophys. Res. Lett.*, **26**, 3193–3196, 1999.

Brace, L. H., W. R. Hoegy, and R. F. Theis, Solar EUV measurements at Venus based on photoelectron emission from the Pioneer Venus Langmuir probe, *J. Geophys. Res.*, **93**, 7282–7296, 1988.

Colburn, D. S., J. D. Mihalov, and C. P. Sonett, Magnetic observations of the lunar cavity, *J. Geophys. Res.*, **76**, 2940–2957, 1971.

Decreau, P. et al. (20 co-authors), Early results from the Whisper instrument on CLUSTER: an overview, *Ann. Geophys.*, submitted, 2001.

Garrett H. B. and A. G. Rubin, Spacecraft charging at geosynchronous orbit-generalized solution for eclipse passage, *Geophys. Res. Lett.*, **5**, 865–868, 1978.

Grobman, W. D. and J. L. Blank, Electrostatic potential distribution of the sunlit lunar surface, *J. Geophys. Res.*, **74**, 3943–3951, 1969.

Gustaffson, G. et al., First results of electric field and density observations by Cluster EFW based on initial months of operation, *Ann. Geophys.*, submitted, 2001.

Hollweg, J. V., Interaction of the solar wind with the Moon and formation of a lunar limb shock wave, *J. Geophys. Res.*, **73**, 7269–7276, 1968.

Kanekal, S. G., D. N. Baker, J. B. Blake, B. Klecker, R. A. Mewaldt, and G. M. Mason, Magnetospheric response to magnetic cloud (coronal mass ejection) events: relativistic electron observations from SAMPEX and Polar, *J. Geophys. Res.*, **104**, 24885–24894, 1999.

Laakso H., Monitoring of the spacecraft potential in space, *J. Atmos. Terr. Phys.*, accepted, 2001.

Laakso H. and M. Jarva, Position and motion of the plasmapause, *J. Atmos. Terr. Phys.*, in press, 2001.

Laakso H. and A. Pedersen, Satellite photoemission characteristics, in *Materials in a Space Environment*, edited by H T D Guyenne, pp. 361–365, ESA SP–368, ESTEC, Noordwijk, 1994.

Laakso H., T. L. Aggson, and R. F. Pfaff, Plasma gradient effects on double probe measurements in the magnetosphere, *Ann. Geophys.*, **13**, 130–146, 1995.

Laakso H. R. Grard, P. Janhunen, and J.-G. Trotignon, Plasma and wave phenomena induced by neutral gas releases in the solar wind, *Ann. Geophys.*, submitted, 2000.

Lin R. P. (8 co-authors), Lunar surface magnetic fields and their interaction with the solar wind: results from Lunar Prospector, *Science*, **281**, 1480–1484, 1998.

Mullen, E. G., M. S. Gussenhoven, D. A. Hardy, T. A. Aggson, B. G. Ledley, and E. Whipple, SCATHA survey of high-level spacecraft charging in sunlight, *J. Geophys. Res.*, **91**, 1474–1490, 1986.

Russell, C. T. and B. R. Lichtenstein, On the source of lunar limb compressions, *J. Geophys. Res.*, **80**, 4700–4711, 1975.

Scudder, J. D., X. Cao, and F. S. Mozer, The photoemission current - spacecraft potential relation: Key to routine, quantitative low-energy plasma measurements, *J. Geophys. Res.*, **105**, 21281–21294, 2000.

Soubeyran, A., Internal and bulk charging: analysis of risks and protection means, in *Space Environment Preventation of Risks Related to Spacecraft Charging*, Cépaduès-Éditions, Toulouse, France, 1996.

Spreiter, J. R., M. C. Marsh, and A. L. Summers, Hydromagnetic aspects of solar wind flow past the Moon, *Cosm. Electrodyn.*, **1**, 5–50, 1970.

Tajmar, M., J. Gonzalez, and A. Hilgers, Modelling of spacecraft-environment interactions on SMART-1, *J. Space. Rockets.*, in press, 2001.